The Activity of Oxidized Bovine Spleen Purple Acid Phosphatase Is Due to an Fe(III)Zn(II) 'Impurity'

ARTICLE *in* BIOCHEMISTRY · AUGUST 1998

Impact Factor: 3.02 · DOI: 10.1021/bi980389r · Source: PubMed

2 AUTHORS:

Maarten Merkx
Technische Universiteit Eindhoven
114 PUBLICATIONS **2,797** CITATIONS
SEE PROFILE

Bruce Averill
George Mason University
171 PUBLICATIONS **5,952** CITATIONS
SEE PROFILE

The Activity of Oxidized Bovine Spleen Purple Acid Phosphatase Is Due to an Fe(III)Zn(II) 'Impurity'

Maarten Merkx and Bruce A. Averill*

E.C. Slater Institute, Biocentrum Amsterdam, University of Amsterdam, Plantage Muidergracht 12, 1018 TV, Amsterdam, The Netherlands

Received February 18, 1998; Revised Manuscript Received June 1, 1998

ABSTRACT: Bovine spleen purple acid phosphatase (BSPAP) is a dinuclear iron protein with two stable redox states. The $Fe^{3+}Fe^{2+}$ state is the active state, while the fully oxidized protein ($BSPAP_{ox}$) has been reported to retain 5−10% activity, corresponding to a k_{cat} of ca. 150 s^{-1} [Dietrich, M., Münstermann, D., Suerbaum, H., and Witzel, H. (1991) *Eur. J. Biochem. 199*, 105−113]. Here we show that this activity does not originate from $Fe^{3+}Fe^{3+}$-BSPAP, but rather from an 'impurity' of FeZn-BSPAP. The FeZn form of BSPAP was prepared from apo-BSPAP following a new procedure, and its kinetic properties were carefully determined for comparison to those of $BSPAP_{ox}$. For the hydrolysis of *p*-NPP at pH 6.00, both k_{cat} and K_M were affected by the Fe^{2+}-to-Zn^{2+}-substitution [$Fe^{3+}Fe^{2+}$-BSPAP, $k_{cat} = (1.8 \pm 0.1) \times 10^3$ s^{-1} and $K_M = 1.2 \pm 0.2$ mM; $Fe^{3+}Zn^{2+}$-BSPAP; $k_{cat} = (2.8 \pm 0.2) \times 10^3$ s^{-1} and $K_M = 3.3 \pm 0.4$ mM]. The K_M of $BSPAP_{ox}$ was the same as that of FeZn-BSPAP. pH profiles of $BSPAP_{ox}$ and FeZn-BSPAP were both shifted to lower pH compared to that of $BSPAP_{red}$. FeZn-BSPAP, FeZn-BSPAP·PO_4, and FeZn-BSPAP·MoO_4 all showed characteristic EPR spectra similar to the corresponding complexes of FeZn-Uf. The same species could also be observed in concentrated samples of native BSPAP. Spin integration of these spectra showed a quantitative relation between the spin concentration of the FeZn-BSPAP 'impurity' and the residual phosphatase activity after oxidation. Since all activity found after oxidation of BSPAP could be attributed to FeZn-BSPAP, there is no direct evidence that $Fe^{3+}Fe^{3+}$-BSPAP is catalytically active. These results set an upper limit to the possible catalytic activity of the $Fe^{3+}Fe^{3+}$ form of ≤1% of that of the $Fe^{3+}Fe^{2+}$ form, a finding that is important for understanding the fundamental chemistry by which these dinuclear enzymes catalyze the hydrolysis of phosphate esters.

Purple acid phosphatases (PAP)[1] are characterized by a low pH optimum (pH 5−6), a purple color, insensitivity to the acid phosphatase inhibitor tartrate, and the presence of a dinuclear FeFe or FeZn center at their active site (*2*−*6*). Purple acid phosphatases, which are sometimes also referred to as tartrate-resistant acid phosphatases (TRAPs) or type 5 acid phosphatases, have been isolated from mammalian sources, including porcine uterine fluid (uteroferrin, Uf) (*7*), bovine spleen (BSPAP) (*8*), and several human and rat tissues (spleen, bone, lung) (*6*), from plants, e.g., red kidney beans (KBPAP) (*9*), sweet potato (*10, 11*), and *Arabidopsis thalania* (cited in ref 6), and from microbial organisms (*12, 13*). The mammalian enzymes, of which Uf and BSPAP are the best-studied examples, contain two antiferromagnetically coupled iron atoms (*1, 14, 15*), while the kidney bean purple acid phosphatase contains one iron and one zinc. Despite this difference in metal content, the mammalian and plant purple acid phosphatases display very similar enzymatic and spectroscopic properties. One of the irons in BSPAP and Uf can be replaced by zinc without drastic effects on the phosphatase activity (*1, 16*−*18*), while the zinc in KBPAP can be replaced by iron, again without major effects on the catalytic activity (*19, 20*). KBPAP is the only PAP whose X-ray structure has been determined (*21, 22*). Although there is little overall sequence homology between KBPAP and the mammalian enzymes, all the metal-coordinating amino acids and some amino acids in the proximity of the dinuclear metal center are conserved among all purple acid phosphatases, suggesting a similarity in active site structure between the FeZn center in KBPAP and the mixed-valent $Fe^{3+}Fe^{2+}$ state of the mammalian enzymes (*23*). The recently reported X-ray structures of two Ser/Thr-specific protein phosphatases (PP's), protein phosphatase 2B (or calcineurin) (*24, 25*) and protein phosphatase 1 (*26, 27*), revealed the presence of a

* To whom correspondence should be addressed. Telephone: 31-20-5255045. Fax: 31-20-5255124. E-mail: BAA@chem.uva.nl.

[1] Abbreviations: AAS, atomic absorption spectrometry; BSA, bovine serum albumin; BSPAP, bovine spleen purple acid phosphatase; $BSPAP_{ox}$, BSPAP after oxidation by hydrogen peroxide; $BSPAP_{red}$, BSPAP in the active, mixed-valent oxidation state; EDTA, disodium salt of ethylenediaminetetraacetic acid; EPR, electron paramagnetic resonance; EXAFS, extended X-ray absorption fine structure; FeFe-BSPAP, BSPAP with iron at the ferric and ferrous sites; FeZn-BSPAP, BSPAP with iron at the ferric site and zinc at the ferrous site; FeZn-$BSPAP_{native}$, FeZn-BSPAP as found in native BSPAP preparations; FeZn-BSPAP·MoO_4, FeZn-BSPAP complexed with molybdate; FeZn-BSPAP·PO_4, FeZn-BSPAP complexed with phosphate; FeZn-Uf, Uf with iron at the ferric site and zinc at the ferrous site; FeZn-Uf·MoO_4, FeZn-Uf complexed with molybdate; FeZn-Uf·PO_4, FeZn-Uf complexed with phosphate; HEPES, *N*-(2-hydroxyethyl)piperazine-*N*′-2-ethanesulfonic acid; KBPAP, purple acid phosphatase of red kidney beans; MES, 2-(*N*-morpholino)ethanesulfonic acid; PAP, purple acid phosphatase; *p*-NPP, disodium salt of *p*-nitrophenyl phosphate; PP, protein phosphatase; PP1, protein phosphatase 1; PP2B, protein phosphatase 2B; $P_{1/2}$, microwave power at half-saturation; SOD, superoxide dismutase; Uf, uteroferrin.

S0006-2960(98)00389-4 CCC: $15.00
Published on Web 07/21/1998

dinuclear metal center with a coordination environment identical to the KBPAP active site, except for the absence of the tyrosinate ligated to Fe^{3+} that gives the PAP's their characteristic purple color. A sequence motif incorporating most of the metal-coordinating amino acids found in the PAP and PP structures has now been identified in a large group of phosphoesterases, including other phosphomonoesterases, diadenosinetetraphosphatase, exonuclease, and 5′-nucleosidases (*28*−*30*). Among all these phosphoesterases, the metal center and catalytic mechanism are probably best characterized for the PAP's.

The active state of the mammalian PAP's is clearly the $Fe^{3+}Fe^{2+}$ oxidation state. Oxidation of the mammalian PAP's to the $Fe^{3+}Fe^{3+}$ state results in a decrease of the phosphatase activity to 5−10% (*31*−*33*), while reduction by dithionite to the diferrous state results in the destruction of the metal center and the release of Fe^{2+} (*16*, *34*). The metal content and active oxidation state of the PP's are still the subject of some debate (*35*). The identification of a superoxide dismutase (SOD) as a factor that protects calcineurin against inactivation lead Klee and co-workers to propose that the $Fe^{2+}Zn^{2+}$ state is the active oxidation state in calcineurin, and that SOD protects the enzyme from inactivation by preventing the oxidation to the $Fe^{3+}Zn^{2+}$ state (*36*). This proposal is in conflict with reports from Rusnak and co-workers, who showed that the strong reductant dithionite inactivated both the native FeZn calcineurin and its FeFe derivative (*37*). Additional EPR redox titrations on the FeFe derivative of calcineurin clearly showed that, as in the purple acid phosphatases, the mixed-valent $Fe^{3+}Fe^{2+}$ state is the catalytically active oxidation state (*38*). As with the PAP's, the activity of FeFe-calcineurin was diminished by the addition of hydrogen peroxide, but not completely abolished. A remarkable difference between the PAP's and calcineurin is their catalytic efficiency as expressed in the turnover number for the hydrolysis of *p*-nitrophenyl phosphate, which is 1800 s^{-1} for BSPAP (*34*) but typically only 26 s^{-1} for calcineurin (*39*).[2]

Assuming that all of the enzymatic activity observed is due to the diferric form, the 5−10% activity remaining after oxidation of BSPAP and Uf by hydrogen peroxide corresponds to a k_{cat} of 100−200 s^{-1}. This value is larger than the k_{cat} values observed for calcineurin, and suggests that the $Fe^{3+}Fe^{3+}$ form itself is a reasonable good catalyst. Dietrich et al. have clearly demonstrated that this $BSPAP_{ox}$ activity does not result from incomplete oxidation of the $Fe^{3+}Fe^{2+}$ cluster, since the EPR spectrum of a concentrated $BSPAP_{ox}$ sample showed the complete absence of the typical $g < 2$ signal characteristic of $Fe^{3+}Fe^{2+}$-BSPAP (*32*). In addition, the pH dependence of $BSPAP_{ox}$ was shown to be different from that of $BSPAP_{red}$. They therefore concluded that the $Fe^{3+}Fe^{3+}$ form of BSPAP was responsible for the catalytic activity. A remarkable finding of their study was that the oxidation of the $Fe^{3+}Fe^{2+}$ form to the $Fe^{3+}Fe^{3+}$ form did not drastically affect the substrate affinity, as similar K_M values were determined for $BSPAP_{ox}$ and $BSPAP_{red}$. Spectroscopic studies, however, showed a much stronger affinity for phosphate for oxidized BSPAP compared to the mixed-valent $Fe^{3+}Fe^{2+}$ state (*31*). Two anion binding sites were therefore postulated for $Fe^{3+}Fe^{3+}$-BSPAP: a 'spectroscopic' site with very high affinity for phosphate, and a 'catalytic' site where substrate binds, with much weaker affinity for oxoanions. An alternative explanation for the PAP_{ox} activity, which has been suggested to explain the activities found after oxidation of Uf (*33*) and the FeFe-substituted form of calcineurin (*38*), is that these phosphatases contain small amounts of an FeZn form, which cannot be inactivated by oxidation. This possibility was considered by Dietrich et al. for BSPAP, but the inability of EDTA to inactivate $BSPAP_{ox}$ was put forward by them as an argument against this explanation. It was expected that EDTA would extract the zinc ion from the divalent metal site, since EDTA was known to extract the zinc ion from KBPAP (*40*).

In this study, we have prepared the FeZn form of BSPAP from apo-BSPAP and carefully characterized its kinetics and its EPR spectroscopic properties. These results were then compared to the corresponding properties of $BSPAP_{ox}$, and demonstrate that BSPAP contains an 'impurity' of FeZn-BSPAP that can account quantitatively for the activity observed after oxidation of BSPAP. The intrinsic catalytic activity of $Fe^{3+}Fe^{3+}$-BSPAP, if any, is therefore less than 1% of the $Fe^{3+}Fe^{2+}$ activity. The implications of this finding for the other PAP's, the PAP catalytic mechanism, and the physiological role of PAP's are discussed.

EXPERIMENTAL PROCEDURES

General. Unless stated otherwise, protein solutions contained 40 mM sodium acetate, 1.6 M KCl, and 20% (v/v) glycerol, pH 5.0. Optical spectra were measured on an HP8452A diode array spectrophotometer. Bovine spleen purple acid phosphatase was isolated as previously described (*34*). Preparations had $A_{280nm}/A_{536\ nm}$ ratios of ∼14. FeZn-BSPAP was prepared as described previously by addition of $FeCl_3$ and $Zn(OAc)_2$ to apo-BSPAP (*34*). Protein determination was done by measuring the absorption of the tyrosinate-to-Fe^{3+} charge-transfer band at 536 nm ($\epsilon = 4080$ $M^{-1}\cdot cm^{-1}$).

Metal Analyses. Metal analyses were performed on a Hitachi 180-80 polarized Zeeman atomic absorption spectrometer equipped with a graphite furnace. Adventitious metal ions were removed from protein and buffer by passage through a Chelex-100 column (Bio-Rad).

Kinetics. Enzyme assays were performed by monitoring the formation of *p*-nitrophenolate at 410 nm from the hydrolysis of *p*-nitrophenyl phosphate. At several times after enzyme addition, 250/500 μL aliquots were taken and quenched by mixing with 1.5 mL of 0.5 M NaOH to convert all product to the phenolate form ($\epsilon = 16.6$ $mM^{-1}\cdot cm^{-1}$). Since BSPAP is partly inactivated in dilute solutions, the enzyme was diluted in 50 mM sodium acetate, 2 M KCl, and 0.5 mg/mL BSA to prevent inactivation. $BSPAP_{ox}$ was prepared by incubation of BSPAP with 2 mM hydrogen peroxide for 10 min at 0 °C, followed by dilution in the 0.5 mg/mL BSA-containing buffer. Specific activities of $BSPAP_{ox}$ and FeZn-BSPAP were measured in a buffer containing 100 mM Na-MES, 200 mM KCl, and 10 mM *p*-NPP, pH 6.00. To prevent oxidation, $Fe(NH_4)_2(SO_4)_2$ (0.2 mM) and ascorbate (15 mM) were added for $BSPAP_{red}$. pH profiles were measured in 100 mM buffer (NaOAc, Na-MES, or Na-HEPES), 200 mM KCl, and 2 or 50 mM *p*-NPP. pH

[2] Calcineurin is activated by Mn^{2+}. The turnover number was obtained in the presence of 1 mM Mn^{2+}.

values were measured immediately at the end of the assay (2 min after the addition of enzyme). For each determination of K_M and V_{max}, the hydrolysis rate was measured at nine different *p*-NPP concentrations between 0.3 and 50 mM. Values of K_M and V_{max} were obtained by a nonlinear fit of the Michaelis−Menten equation using the program Enzyme-Kinetics (Trinity Software).

EPR Spectroscopy. X-band EPR spectra (9.43 GHz) were obtained on a Bruker ECS106 EPR spectrometer, equipped with an Oxford Instruments ESR900 helium-flow cryostat with an ITC4 temperature controller. Spectra at 77 K were measured in a quartz dewar filled with liquid nitrogen. The magnetic field was calibrated with an AEG Magnetic Field Meter. The frequency was measured with an HP 5350B Microwave Frequency Counter.

EPR spectra of high-spin ferric complexes were analyzed using the spin Hamiltonian:

$$H = H_{\text{Zeeman}} + H_{\text{zero field}} \quad (1)$$

where $H_{\text{zero field}} = D[S_z^2 - {}^1/_3(S(S+1)) + (E/D)(S_x^2 - S_y^2)]$ and $H_{\text{Zeeman}} = \beta_e S_0 g_0 B$.

In the weak-field regime, when $|D| \geq \beta_e S_0 g_0 B$, values for g_{eff} depend only on E/D and are frequency-independent (*41*, *42*). The EPR spectrum of a high-spin ferric complex can then be analyzed in terms of the E/D value(s) of the species responsible for the EPR spectrum. We used the program RHOMBO for this analysis (*42*).

Spin quantitation was performed by direct double integration of the FeZn-BSPAP·PO_4 spectra[3] and a Cu^{2+} standard (9.88 mM $CuSO_4$, 2 M $NaClO_4$, 10 mM HCl), both collected at 30 K (*43*, *44*). It was assumed that the Kramers doublet that corresponds to the $g = 4.3$ signal ($|\pm 3/2\rangle$) was fully populated at 30 K, as changing the temperature between 4 and 8 K had only small effects on the intensities of both the $g = 4.3$ and the $g = 9.6$ signals, indicating a low value of the zero-field splitting parameter D ($|D| \leq 1$ cm^{-1}).

EPR Titrations of Anion Binding. The phosphate complexes were prepared by the addition of small amounts of 50 mM and 1.00 M stock solutions of KH_2PO_4 in Millipore water. The molybdate complexes were prepared by the addition of small amounts of 2 and 5 mM stock solutions of Na_2MoO_4 in Millipore water, pH ~8. After characterization by EPR of the unligated protein, the sample was thawed, and an aliquot of a concentrated stock solution of the anion was added. The sample was thoroughly mixed and frozen again in liquid nitrogen, and a new spectrum was obtained. This process was repeated, and spectra were obtained for several anion concentrations. Anion concentrations and spectral amplitudes were corrected for the subsequent dilutions taking place.

Equation 2 was used to analyze the titration data.

$$K_d = [E_{\text{free}}][L_{\text{free}}]/[EL] \quad (2)$$

For phosphate binding, where the protein concentration is small compared to the K_d and $[L]_{\text{free}} \approx [L]_{\text{total}}$, eq 2 can be rewritten as eq 3:

$$[EL] = [E_{\text{total}}][L_{\text{total}}]/(K_d + [L_{\text{total}}]) \quad (3)$$

For molybdate binding, where the protein concentration is comparable or high compared to K_d, eq 2 can be rewritten as

$$K_d = \{([E_{\text{total}}] - [EL])([L_{\text{total}}] - [EL])\}/[EL] \quad (4)$$

$$[EL]^2 - ([L_{\text{total}}] + [E_{\text{total}}] + K_d)[EL] + [L_{\text{total}}][E_{\text{total}}] = 0 \quad (5)$$

$$2[EL] = -([L_{\text{total}}] + [E_{\text{total}}] + K_d) + \{(-[L_{\text{total}}] - [E_{\text{total}}] - K_d)^2 - 4[L_{\text{total}}][E_{\text{total}}]\}^{1/2} \quad (6)$$

with EL = enzyme−ligand complex; E_{free} = unligated enzyme; E_{total} = total amount of enzyme; L_{free} = nonbound ligand; L_{total} = total amount of ligand.

Equations 3 and 6 were fitted using a nonlinear least-squares fit procedure using the program Igor (WaveMetrics) to obtain values for K_d.

RESULTS

The goal of this study was to establish whether the residual activity of $BSPAP_{ox}$ originates from Fe^{3+}-Fe^{3+}-BSPAP or from an 'impurity' of FeZn-BSPAP (which is insensitive to oxidation) in native BSPAP. FeZn-BSPAP was prepared in order to compare its properties with those of $BSPAP_{ox}$. FeZn-BSPAP was obtained by the addition of Fe^{3+} and Zn^{2+} to apo-BSPAP (*34*). FeZn-BSPAP prepared in this way showed a tyrosinate-to-Fe^{3+} charge-transfer band at ~530 nm with an extinction coefficient which is only slightly lower than the 4080 M^{-1}·cm^{-1} of the native enzyme. It contained 1.09 ± 0.09 mol of Fe and 0.96 ± 0.03 mol of Zn per mole of protein. Its specific activity was higher than that of native FeFe-BSPAP and was not affected by the addition of 2 mM hydrogen peroxide, which is consistent with the replacement of the ferrous iron by zinc (*34*). Table 1 shows that both K_M and k_{cat} for the hydrolysis of *p*-nitrophenyl phosphate at pH 6.00 are affected by the Fe^{2+}-to-Zn^{2+} replacement. This is in contrast to previous studies, which reported the same kinetic parameters for $Fe^{3+}Zn^{2+}$-PAP and $Fe^{3+}Fe^{2+}$-PAP (*1*, *18*).

The EDTA insensitivity of $BSPAP_{ox}$ was used by Dietrich et al. to rule out the possibility that the activity of $BSPAP_{ox}$ originated from a small fraction of FeZn-BSPAP, as they expected EDTA to extract the divalent zinc ion (*32*). They also reported the inactivation of $Fe^{3+}Fe^{2+}$-BSPAP upon incubation with 0.1 M EDTA. We incubated FeZn-BSPAP (0.37 μM) in a solution containing 50 mM sodium acetate and 2 M KCl, pH 5.0, both in the presence and in the absence of 0.10 M EDTA. At several times, aliquots were taken, and their activity was determined (10 mM *p*-NPP, 100 mM Na-MES, 200 mM KCl, pH 6.0, 22 °C). The sample without EDTA had a specific activity of 42 ± 1 units/mL, while the specific activity of the EDTA containing sample was 41 ± 1 units/mL. No inactivation was observed for up to 3 h. This finding is in marked contrast to results obtained with KBPAP, where incubation with EDTA has been reported to result in the abstraction of Zn^{2+} from the active site (*40*). In contrast to the results of Dietrich et al. (*32*), we found that inactivation of $Fe^{3+}Fe^{2+}$-BSPAP by EDTA is not observed

[3] The abbreviations PO_4 and MoO_4 are used without specifying the actual state of protonation of these oxoanions.

Table 1: Kinetic Parameters for the Hydrolysis of *p*-NPP by $BSPAP_{Red}$, $BSPAP_{ox}$, and FeZn-BSPAP[a]

enzyme	K_M (mM)	$k_{cat} \times 10^{-3}$ (s^{-1})
$BSPAP_{red}$ [b]	1.2 (0.2)	1.8 (0.1)
$BSPAP_{ox}$ [c]	3.7 (0.4)	0.28 (0.02)
FeZn-BSPAP [c]	3.3 (0.4)	2.8 (0.2)

[a] Numbers in parentheses are standard deviation values. k_{cat} is defined as the number of substrate molecules hydrolyzed per enzyme molecule per second. [b] Assays were performed at 22 °C and pH 6.0 in a buffer containing 100 mM Na-MES, 200 mM KCl, 15 mM ascorbate, and 0.2 or 2 mM $Fe(NH_4)_2(SO_4)_2$. [c] Assays were performed at 22 °C and pH 6.0 in a buffer containing 100 mM Na-MES and 200 mM KCl.

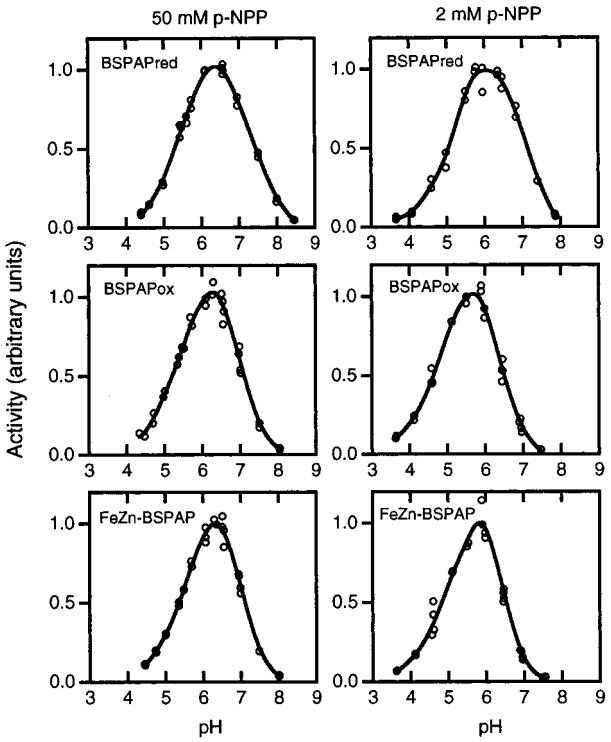

FIGURE 1: pH dependences of $BSPAP_{red}$ (top), $BSPAP_{ox}$ (middle), and FeZn-BSPAP (bottom) at 50 mM *p*-NPP (left) and 2 mM *p*-NPP (right) at 22 °C. Assays for $BSPAP_{red}$ were performed in 100 mM buffer (Na-salt), 200 mM KCl, 15 mM ascorbate, and 0.2 mM $Fe(NH_4)_2(SO_4)_2$. Assays for $BSPAP_{ox}$ and FeZn-BSPAP were performed in 100 mM buffer (Na-salt) and 200 mM KCl. Activities are in arbitrary units and were scaled to obtain the same maximal activities for all profiles (the maximum activity at the pH optimum was as follows: $BSPAP_{red}$/50 mM *p*-NPP, 2930 units/mg; $BSPAP_{red}$/2 mM *p*-NPP, 1690 units/mg; $BSPAP_{ox}$/50 mM *p*-NPP, 275 units/mg; $BSPAP_{ox}$/2 mM *p*-NPP, 164 units/mg; FeZn-BSPAP/50 mM *p*-NPP, 4380 units/mg; FeZn-BSPAP/2 mM *p*-NPP, 1670 units/mg). The solid lines were drawn for illustration purposes only and do not represent a theoretical fit.

when the activity assay is carried out in the presence of a reductant (Fe^{2+}/ascorbate).

Although the activity of $BSPAP_{ox}$ is only 5−10% that of $BSPAP_{red}$, similar K_M values and inhibition constants have been reported for both $BSPAP_{ox}$ and $BSPAP_{red}$ (*32*). The pH optimum of $BSPAP_{ox}$ was reported to be shifted to lower pH values relative to that of $BSPAP_{red}$. Table 1 compares the K_M values for $BSPAP_{red}$, $BSPAP_{ox}$, and FeZn-BSPAP for the hydrolysis of *p*-NPP at pH 6.0. The K_M values of FeZn-BSPAP and $BSPAP_{ox}$ are identical and significantly higher than that observed for $BSPAP_{red}$. Figure 1 shows the pH dependences of $BSPAP_{red}$, $BSPAP_{ox}$, and FeZn-BSPAP at 50 and 2 mM *p*-NPP. At 50 mM *p*-NPP, where the pH profiles represent mainly the effect of pH on V_{max}, the pH optimum is at pH 6.3 for all three BSPAP forms. The $BSPAP_{red}$ profile is broader, however, and extends to higher pH compared to both $BSPAP_{ox}$ and FeZn-BSPAP, which display identical pH profiles. At 2 mM *p*-NPP, where the pH profiles represent pH effects on both V_{max} and K_M, the same trends can be observed. The apparent pK_a of the basic limb is at 7.2 for $BSPAP_{red}$ and at 6.5 for both $BSPAP_{ox}$ and FeZn-BSPAP. Qualitatively, these trends for $BSPAP_{ox}$ and $BSPAP_{red}$ are the same as those reported by Dietrich et al. using 10 mM α-naphthyl phosphate as the substrate (*32*).

Table 2: Zinc Content and Activity after Hydrogen Peroxide Treatment for Three Native BSPAP Batches and FeZn-BSPAP

batch	[protein] (μM)[a]	[Zn] (μM)[b]	[Zn]/[protein]	activity (units/mL)[c]	activity/[Zn] (units/nmol)
BSPAP #1	89	10.1	0.11	800	80
BSPAP #2	88	10.4	0.12	1120	108
BSPAP #3	101	14.7	0.15	1330	91
FeZn-BSPAP	166	156	0.94	21600	138

[a] Protein concentration was determined by measuring $A_{536\ nm}$ with $\epsilon_{536\ nm} = 4080\ M^{-1}\cdot cm^{-1}$. [b] Determined by AAS using Chelex-100-treated enzyme. [c] Activity after incubation with 2 mM H_2O_2 (10 min; 0 °C) in 100 mM Na-MES, 200 mM KCl, 10 mM *p*-NPP, pH 6.0.

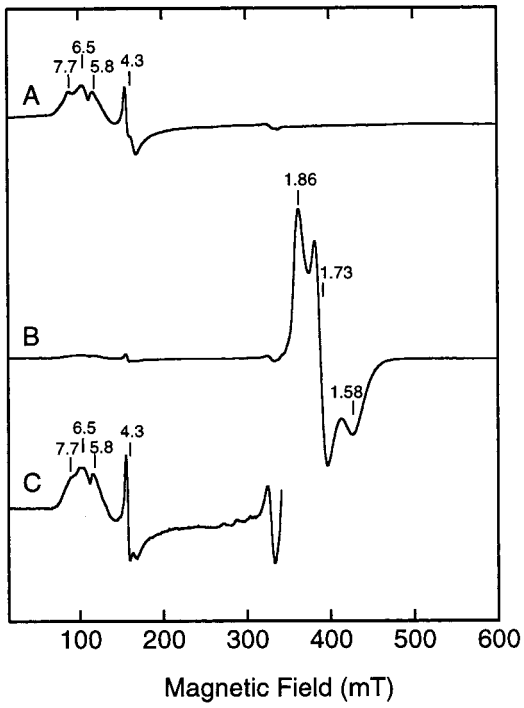

FIGURE 2: EPR spectra of (A) FeZn-BSPAP (166 μM) and (B, C) FeFe-BSPAP (667 μM). The amplitudes of (A) and (B) were corrected for differences in instrument gain, protein concentration, and tube dimensions between the two samples. Spectrum C is spectrum B after 15-fold enlargement. Buffer: 40 mM sodium acetate, 1.6 M KCl, and 20% (v/v) glycerol, pH 5.0. EPR conditions: microwave power, 2.0 mW; microwave frequency, 9.43 GHz; modulation, 12.7 G at 100 kHz; temperature, 4.1 K.

The inability of EDTA to inactivate FeZn-BSPAP, the identical K_M values for $BSPAP_{ox}$ and FeZn-BSPAP, and the identical pH dependence for $BSPAP_{ox}$ and FeZn-BSPAP all indicated that native BSPAP might contain an 'impurity' of FeZn-BSPAP. To see whether BSPAP preparations contained sufficient amounts of zinc to account for the residual activity after oxidation, the zinc content and the activity of $BSPAP_{ox}$ were determined for three different preparations

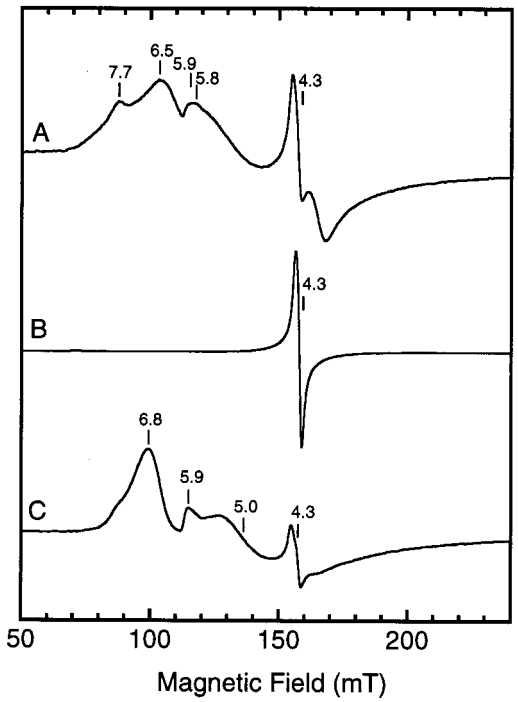

FIGURE 3: EPR spectra of (A) FeZn-BSPAP, (B) FeZn-BSPAP·PO_4, and (C) FeZn-BSPAP·MoO_4. The spectra were normalized to give similar signal heights. Buffer: 40 mM sodium acetate, 1.6 M KCl, and 20% (v/v) glycerol, pH 5.0. EPR conditions: microwave frequency, 9.43 GHz; modulation, 12.7 G at 100 kHz. FeZn-BSPAP: 0.17 mM protein; microwave power, 0.502 mW; temperature, 4.1 K. FeZn-BSPAP·PO_4: 0.15 mM protein and 94 mM KH_2PO_4; microwave power, 7.96 mW; temperature, 30 K. FeZn-BSPAP·MoO_4: 0.13 mM protein and 505 μM Na_2MoO_4; microwave power, 0.502 mW; temperature, 4.9 K.

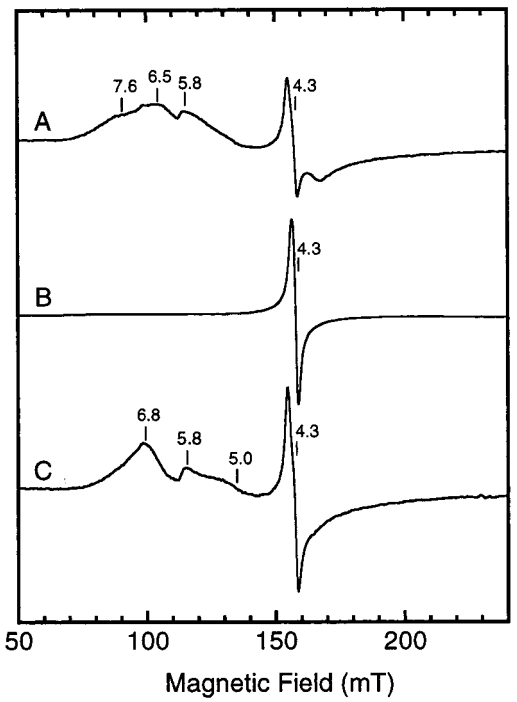

FIGURE 4: EPR spectra of (A) FeZn-$BSPAP_{native}$, (B) FeZn-$BSPAP_{native}$·PO_4, and (C) FeZn-$BSPAP_{native}$·MoO_4. The spectra were normalized to give similar signal heights. Buffer: 40 mM sodium acetate, 1.6 M KCl, and 20% (v/v) glycerol, pH 5.0. EPR conditions: microwave frequency, 9.43 GHz; modulation, 12.7 G at 100 kHz. FeZn-$BSPAP_{native}$: 0.67 mM protein; microwave power, 0.502 mW; temperature, 4.1 K. FeZn-$BSPAP_{native}$·PO_4: 0.63 mM protein and 48 mM KH_2PO_4; microwave power, 12.6 mW; temperature, 30 K. FeZn-$BSPAP_{native}$·MoO_4: ~0.5 mM protein and 0.88 mM Na_2MoO_4; microwave power, 0.502 mW; temperature, 4.9 K.

of BSPAP. Table 2 shows that these BSPAP batches contained 0.10−0.15 mol of zinc per mole of protein. Specific activities after oxidation by hydrogen peroxide ranged from 80 to 108 units/nmol of Zn. Since these values are all lower than the specific activity of FeZn-BSPAP (138 units/nmol of Zn), the zinc content is indeed sufficient to account for the $BSPAP_{ox}$ activity in all three BSPAP batches.

The kinetic parameters and metal content of $BSPAP_{ox}$ are consistent with the presence of an FeZn-BSPAP 'impurity' in preparations of native FeFe-BSPAP, but they do not constitute conclusive evidence. A concentrated sample of (native) FeFe-BSPAP (0.67 mM) was therefore prepared to see if the EPR signal characteristic of FeZn-BSPAP could be detected. Figure 2 shows the EPR spectra of FeZn-BSPAP and native BSPAP at EPR conditions (microwave power, temperature) that are optimal for the native enzyme. The spectrum of FeZn-BSPAP consists of several features at $g = 7.6$, 6.5, 5.8, and 4.3 that are consistent with high-spin Fe^{3+}. The characteristic EPR signal of Fe^{3+}-Fe^{2+}-BSPAP at $g = 1.86$, 1.73, and 1.58 is totally absent in the FeZn-BSPAP sample. At the position of the FeZn-BSPAP signal, the spectrum of native BSPAP shows a weak peak at $g = 4.3$ along with a very weak, broad feature between $g = 10$ and $g = 5$. 15-fold enlargement of this feature (Figure 2C) reveals a spectrum that is very similar to that of FeZn-BSPAP, providing spectroscopic evidence for the presence of FeZn-BSPAP in native BSPAP preparations. We will refer to this species as FeZn-$BSPAP_{native}$.

Figure 3A shows the EPR spectrum of FeZn-BSPAP in more detail. The spectrum shows peaks that belong to several high-spin Fe^{3+} species with different rhombicities. The signal at $g = 6.5$ belongs to the ground doublet of a species with $E/D \sim 0.02$, and that at $g = 5.9$ to the middle Kramers doublet of the same species. A more rhombic species with $E/D \sim 0.08$ is responsible for the peaks at $g = 7.7$ (ground doublet) and $g = 5.8$ (middle doublet). The third species that can be readily observed is the sharp $g = 4.3$ signal of a high-spin Fe^{3+} in a rhombic environment ($E/D \sim 0.33$). It has been proposed by several studies that the ferric iron in PAP coordinates a water ligand with a pK_a around 4.5 (*32*, *45*−*47*). To determine whether the two major components in the FeZn-BSPAP spectrum ($E/D = 0.02$ and 0.08, vide infra) correspond to the water and hydroxide ligated FeZn centers, spectra were measured at pH 4.2, 5.2, and 5.91, but no clear differences were detected (spectra not shown). The spectrum does not show any sign of temperature broadening up to 30 K.[4] The EPR spectrum of FeZn-Uf has also been shown to be composed of several high-spin Fe^{3+} species with various rhombicities (*18*). Based on the relative intensities of the various peaks, these authors concluded that the $g = 4.3$ signal, which is more prominent in the FeZn-Uf spectrum than in our FeZn-BSPAP spectrum, represented the majority of the high-spin Fe^{3+}. The nearly isotropic signal at $g = 4.3$ is much sharper than the broad

[4] This behavior is in contrast to that reported earlier for FeZn-BSPAP, but very similar to FeZn-Uf. The previously reported FeZn-BSPAP was, however, prepared via a different procedure and utilized the so-called low-salt form of BSPAP (*1*).

and anisotropic signals of the species with $E/D = 0.02$ and $E/D = 0.08$, however, making it easy to overestimate the contribution of this species to the spectrum. The integrated spectrum of Figure 3A (not shown) indicates that the $g = 4.3$ signal represents only a small fraction of the total EPR-detectable iron. The majority of the high-spin Fe^{3+} is therefore represented by the more axial species. The broadness of these features, which may result from a combination of E/D strain, g-strain, and the anisotropic nature of the spectra, may have precluded their detection in previous EPR studies on BSPAP. It also makes spin integration of the various species (or their sum) difficult.

Figure 4A shows the FeZn-$BSPAP_{native}$ spectrum as observed in the concentrated native BSPAP sample. Although not identical to the FeZn-BSPAP spectrum, it consists of the same principal components. As with FeZn-BSPAP, peaks can be detected at $g = 7.6$, 6.5, 5.8−5.9, and 4.3, which correspond to species with $E/D = 0.08$, $E/D = 0.02$, and $E/D = 0.33$. An additional, very weak peak can be observed at $g = 6.8$, which corresponds to an E/D of ∼0.035. The saturation behavior of FeZn-BSPAP and FeZn-$BSPAP_{native}$ is the same, both at 4 K and at 30 K.

Figure 3B shows the EPR spectrum of the phosphate complex of FeZn-BSPAP. The FeZn-BSPAP·PO_4 spectrum shows an intense $g = 4.3$ signal corresponding to the middle Kramers doublet of high-spin Fe^{3+} in a rhombic environment ($E/D \sim 0.33$). A small peak at $g = 9.6$ (∼100 times weaker), corresponding to transitions in the lowest and highest doublets, is also observed. This spectrum is very similar to the EPR spectrum of FeZn-Uf·PO_4 (*18*). The titration experiment in Figure 5 nicely shows the conversion of the broad signal of FeZn-BSPAP into the sharp signal at $g = 4.3$ of FeZn-BSPAP·PO_4 (note the different intensities for the broad $5 < g < 10$ feature and the sharp $g = 4.3$ signal). Both the $E/D = 0.02$ and the $E/D = 0.08$ species are affected simultaneously and similarly by the addition of phosphate, confirming that both species belong to iron in the FeZn active site. Fits of the signal intensities at $g = 6.5$ and $g = 4.3$ as a function of phosphate concentration gave K_d values of 8 ± 2 and 9.3 ± 0.6 mM, respectively. The addition of phosphate to the native BSPAP sample converts the FeZn-$BSPAP_{native}$ EPR signal to the same sharp $g = 4.3$ signal observed for FeZn-BSPAP·PO_4 (Figure 4B). Phosphate titration experiments were also performed in the absence of glycerol (in 50 mM sodium acetate, 2 M KCl, pH 5.0; not shown). K_d values of ∼1 mM for both FeZn-BSPAP and FeZn-$BSPAP_{native}$ were obtained, indicating similar affinities for phosphate for both species. Removal of the phosphate by several dilution/concentration steps with phosphate-free buffer resulted in the original FeZn-BSPAP EPR spectra, showing that the effect of phosphate on the EPR spectra is reversible.

The EPR spectra of the FeZn-BSPAP·PO_4 complexes are nearly isotropic, which facilitates their integration and the determination of spin concentrations. Spin concentrations of 161 and 38.3 μM were calculated for the FeZn-BSPAP and the FeZn-$BSPAP_{native}$ samples, respectively. Activity measurements of both EPR samples after oxidation by hydrogen peroxide gave specific activities of 134 units/(nmol of $g = 4.3$ Fe^{3+}) for FeZn-BSPAP and 128 units/(nmol of $g = 4.3$ Fe^{3+}) for FeZn-$BSPAP_{native}$. In other words, the amount of FeZn-BSPAP detected by EPR for the native enzyme corresponds quantitatively to the activity found after oxidation. The activity of $Fe^{3+}Fe^{3+}$-BSPAP, if any, is therefore less than 1% of the activity of $Fe^{3+}Fe^{2+}$-BSPAP.

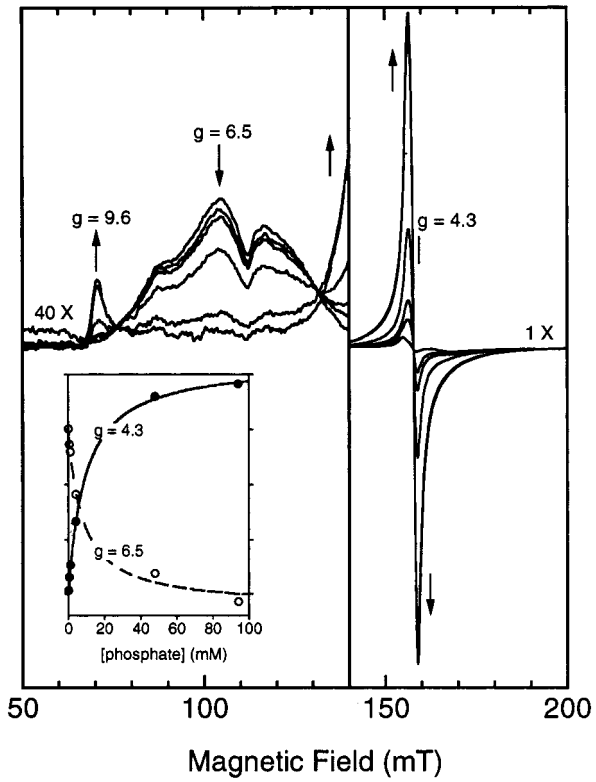

FIGURE 5: EPR titration showing the conversion from FeZn-BSPAP to FeZn-BSPAP·PO_4. Spectra were collected at 0, 0.54, 1.1, 4.2, 48, and 94 mM KH_2PO_4 and ∼0.16 mM protein in 40 mM sodium acetate, 1.6 M KCl and 20% (v/v) glycerol, pH 5.0. The arrows indicate increasing phosphate concentration. EPR conditions: microwave power, 7.96 mW; microwave frequency, 9.43 GHz; modulation, 12.7 G at 100 kHz; temperature, 30 K. Inset: intensities of the $g = 6.5$ and $g = 4.3$ signals as a function of phosphate concentration. Curves describe best fits of eq 3 under Experimental Procedures.

Anion inhibitors of PAP can be divided into two classes. The first consists of phosphate and arsenate, which show (mixed) competitive inhibition with K_i's in the millimolar range, have similar effects on the EPR spectra of FeFe-PAP and FeZn-PAP, and enhance the oxidation of $Fe^{3+}Fe^{2+}$-PAP. The second class consists of molybdate and tungstate, which show noncompetitive inhibition with K_i's in the micromolar range, have similar (but different from phosphate) effects on the EPR spectra of FeFe-PAP and FeZn-Uf, and stabilize the $Fe^{3+}Fe^{2+}$ state of PAP against oxidation (*18, 48*−*50*). The EPR spectrum of FeZn-Uf·MoO_4 was reported to be different from those of FeZn-Uf and FeZn-Uf·PO_4, consisting (mainly) of a species with g-values at 6.92, 5.85, and 5.06, corresponding to $E/D = 0.04$. Figure 3C shows that the EPR spectrum of FeZn-BSPAP·MoO_4 is very similar to that of FeZn-Uf·MoO_4, with g-values at 6.79, 5.86, and 5.01 (E/D ∼ 0.035). The titration experiment in Figure 6 shows the conversion of FeZn-BSPAP to FeZn-BSPAP·MoO_4. Again, both the $E/D = 0.02$ and the $E/D = 0.08$ species are affected simultaneously and similarly by the addition of molybdate, confirming that both species belong to iron in the FeZn active site. A fit of the difference between the $g = 6.8$ intensity and the $g = 6.0$ intensity as a function of molybdate concentration gave a K_d value of 12 ± 3 μM and [FeZn-

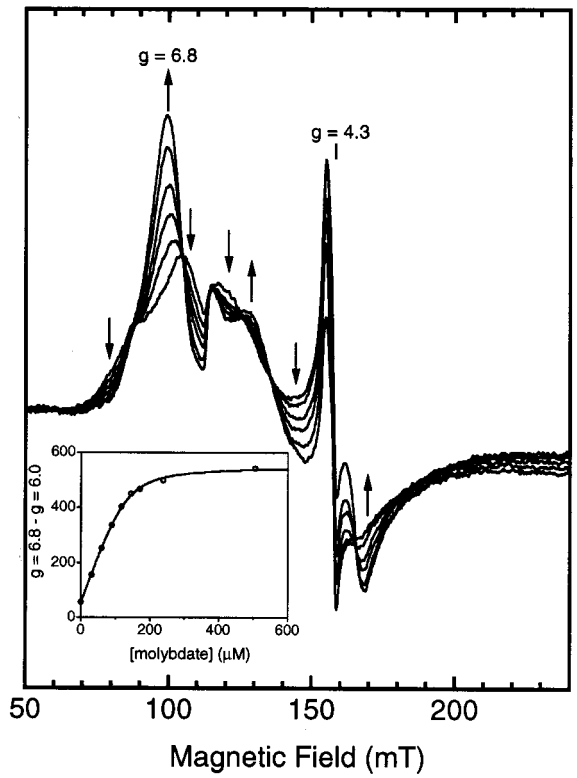

FIGURE 6: EPR titration showing the conversion from FeZn-BSPAP to FeZn-BSPAP·MoO_4. Spectra were collected at 0, 31, 61, 90, 145, and 506 μM Na_2MoO_4 and ~0.13 mM protein in 40 mM sodium acetate, 1.6 M KCl, and 20% (v/v) glycerol, pH 5.0. The arrows indicate increasing molybdate concentration. EPR conditions: microwave power, 7.96 mW; microwave frequency, 9.43 GHz; modulation, 12.7 G at 100 kHz; temperature, 30 K. Inset: the difference of the signal intensities between $g = 6.8$ and $g = 6.0$ as a function of molybdate concentration. The solid line describes the best fit of eq 6 under Experimental Procedures.

BSPAP] = 130 ± 6 μM. Removal of the molybdate by several dilution/concentration steps with molybdate-free buffer resulted in the original FeZn-BSPAP EPR spectrum, showing that the effect of molybdate on the EPR spectrum is also reversible.

Figure 4C shows the EPR spectrum of FeZn-$BSPAP_{native}$·MoO_4. This spectrum is again very similar to the FeZn-BSPAP·MoO_4 spectrum, confirming our identification of these high-spin Fe^{3+} signals as originating from FeZn-BSPAP. The only difference between Figure 3C and Figure 4C is the height of the $g = 4.3$ signal, which is more intense for FeZn-$BSPAP_{native}$·MoO_4. This corresponds to only a small amount of the total iron and is probably due to the release of some iron from denatured BSPAP that may have formed during the repetitive freezing and thawing of the sample. The $g = 4.3$ signal is probably not due to FeZn-BSPAP·PO_4, since it is not affected by the addition of molybdate, which we would expect to replace the less strongly bound phosphate.

DISCUSSION

In this paper, we demonstrate that the phosphatase activity that remains after treatment of BSPAP with hydrogen peroxide is due to a small 'impurity' of FeZn-BSPAP. The following evidence for this assignment is provided: (1) both the K_M value and the pH dependence of $BSPAP_{ox}$ are identical to those of FeZn-BSPAP, while small but significant differences in the K_M and the pH dependence are detected for $BSPAP_{red}$; (2) BSPAP preparations contain sufficient amounts of zinc (0.1−0.15 Zn per protein) to account for the $BSPAP_{ox}$ activity if it is attributed to FeZn-BSPAP; (3) careful inspection of the EPR spectrum of native BSPAP reveals the presence of an EPR signal that is very similar to that of FeZn-BSPAP; (4) the binding of phosphate and molybdate to FeZn-BSPAP and FeZn-$BSPAP_{native}$ results in the same characteristic EPR spectra; (5) spin quantitation of the FeZn-BSPAP·PO_4 and FeZn-$BSPAP_{native}$·PO_4 spectra shows a quantitative relationship between the spin concentration of FeZn-$BSPAP_{native}$ and $BSPAP_{ox}$ activity.

Residual phosphatase activity (3−10%) after oxidation of PAP's has been observed by several groups both for BSPAP (*32, 51*) and for Uf (*33*). Dietrich et al. showed that this activity is not due to residual $Fe^{3+}Fe^{2+}$-BSPAP, since a concentrated $BSPAP_{ox}$ sample showed no $g < 2$ signal. They also observed a shift in the pH dependence for $BSPAP_{ox}$ compared to that of $BSPAP_{red}$. The EDTA insensitivity of $BSPAP_{ox}$ was used by Dietrich et al. as an argument against the possibility that the activity of $BSPAP_{ox}$ originated from a small fraction of FeZn-BSPAP, as they expected EDTA to extract the divalent Zn^{2+} ion. We found that FeZn-BSPAP is not inactivated by EDTA, but we did find EDTA to inactivate $Fe^{3+}Fe^{2+}$-BSPAP. Our observation that this inactivation is not observed in the presence of Fe^{2+}/ascorbate in the assay mixture suggests that EDTA does not extract Fe^{2+} (or Zn^{2+}) from the active site, but may enhance its oxidation to Fe^{3+}. To account for the very different affinities for various oxoanions such as phosphate as determined by kinetic measurements and spectroscopic measurements, two anion binding sites had to be postulated by Dietrich et al. The binding of phosphate at the 'spectroscopic site' was very strong and elicited changes in the optical spectra, but did not affect catalysis. The binding of anion inhibitors (and substrate) at the second site was responsible for the inhibition of catalysis and was much weaker (but similar for $BSPAP_{red}$ and $BSPAP_{ox}$). Our identification of the $BSPAP_{ox}$ activity as originating from FeZn-BSPAP explains the different affinities for oxoanions as observed via kinetic and optical measurements on $BSPAP_{ox}$ without the need to postulate two oxoanion binding sites. A minority species, the FeZn-$BSPAP_{native}$ form, is responsible for the kinetics, while the optical spectra are dominated by the major species present, $Fe^{3+}Fe^{3+}$-BSPAP. These and other activity studies on oxidized PAP's should therefore now be reinterpreted, as they reflect properties of FeZn-PAP and not of $Fe^{3+}Fe^{3+}$-PAP.

Although this report and the study of Dietrich et al. both used BSPAP, our findings are probably also relevant to other members of the mammalian PAP's. This is supported by the fact that various spectroscopic studies, both on BSPAP and on Uf, have reported the presence of small impurities with high-spin Fe^{3+}. Small $g = 4.3$ signals have been reported in several EPR studies on Uf (*18, 52−54*) and BSPAP (*1, 32, 50*). In a study on the binding of phosphate to Uf, EPR spectra showed the appearance of a sharp feature at $g = 4.3$ upon addition of phosphate (*54*). In hindsight, this finding indicates that this $g = 4.3$ signal originated from the phosphate complex of an FeZn-Uf 'impurity'. Magnetic susceptibility studies of PAP's have also reported the

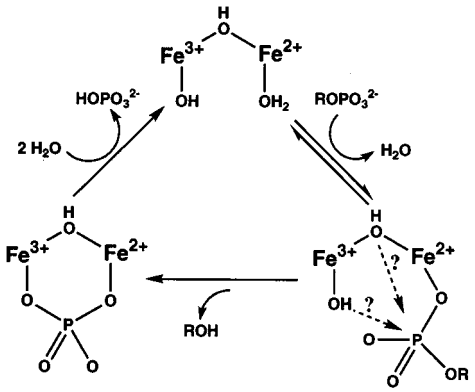

FIGURE 7: Hypothesis for the role of the metal center in the enzymatic mechanism of bovine spleen purple acid phosphatase.

presence of small amounts of high-spin Fe^{3+} (*1*, *14*, *54*, *55*). We would expect that a more careful analysis of the $g = 10$ to $g = 5$ region of the EPR spectrum of Uf and other mammalian PAP's and their anion complexes will also reveal the presence of FeZn-PAP in these preparations.

The EPR spectra of FeZn-BSPAP and its phosphate and molybdate complexes are very similar to those of FeZn-Uf and its corresponding anion complexes. This finding suggests the presence of similar structures for the FeZn-BSPAP and FeZn-Uf active sites and indicates that the results of various spectroscopic studies on FeZn-Uf [EPR, Raman (*18*), EXAFS (*56*), Mössbauer (*57*)] are probably also applicable to FeZn-BSPAP. Thus, David and Que observed a line broadening effect on the EPR spectrum of FeZn-Uf·PO_4 when using $P^{17}O_4$ (originating from unresolved superhyperfine interaction between the $I = 5/2$ nuclear spin of ^{17}O and the electron spin), providing evidence for the direct coordination of phosphate to the iron. The high similarity between the EPR spectra of FeZn-BSPAP and its anion complexes and those of FeZn-Uf and its anion complexes strongly suggests that phosphate also binds directly to the iron in FeZn-BSPAP.

The strong similarity between the EPR spectra of FeZn-BSPAP and FeZn-$BSPAP_{native}$ and their anion complexes, as well as their identical kinetic properties, confirms our previous finding that the relatively small differences in activity that have been detected between $Fe^{3+}Zn^{2+}$-BSPAP and $Fe^{3+}Fe^{2+}$-BSPAP (and also between $Fe^{3+}Fe^{2+}$-BSPAP, $Ga^{3+}Fe^{3+}$-BSPAP, and $Ga^{3+}Zn^{2+}$-BSPAP) (*34*) are significant and not the result of an artifact introduced by their preparation.

Since all activity found after oxidation of BSPAP can be attributed to FeZn-BSPAP, the present work provides no evidence in support of the contention that $Fe^{3+}Fe^{3+}$-BSPAP has catalytic activity. Because it has been impossible to date to prepare the FeFe enzyme free of contamination by the FeZn form, we can, however, only state that the intrinsic activity of the $Fe^{3+}Fe^{3+}$ form is $\leq$1% of that of the Fe^{3+}-Fe^{2+} form. This finding is important for the understanding of the mechanism by which PAP's, and possibly also other phosphoesterases with similar dinuclear metal centers, catalyze the hydrolysis of phosphate esters. The current hypothesis for the catalytic mechanism is shown in Figure 7 (*22*). In the first step, the substrate coordinates to the divalent metal in what is thought to be a fast process (*47*). The substrate is now in an ideal position to be attacked by a hydroxide nucleophile, which in principle can be either the nonbridging hydroxide, coordinated to the ferric iron, or the hydroxide that bridges both metal ions. The hydrolysis is known to occur with inversion of the configuration around the phosphorus, providing strong evidence for direct attack of water on the substrate (*58*). In the final step, the phosphate is released. In principle, the inactivity of $Fe^{3+}Fe^{3+}$-BSPAP may result from an inability to bind substrate. The structure of the oxidized state is unknown and may differ significantly from that of the mixed-valent state. This explanation is less likely, however, since it is well-known from optical spectroscopy (*32*, *49*) and EXAFS (*59*, *60*) that $Fe^{3+}Fe^{3+}$-BSPAP does bind phosphate and other oxoanions such as arsenate, tungstate, and molybdate. In fact, phosphate binding to Fe^{3+}-Fe^{3+}-BSPAP is so strong that gel filtration chromatography is not able to remove the phosphate from $Fe^{3+}Fe^{3+}$-BSPAP·PO_4. $Fe^{3+}Fe^{3+}$-BSPAP is therefore probably still able to bind substrate (*31*). Whether the subsequent hydrolysis step still takes place remains to be established. But even if it does, the bridging phosphate complex that is then formed is likely to be so stable that the enzyme can no longer release phosphate and participate in another catalytic cycle.

It is not clear whether the FeZn-BSPAP 'impurity' is also present in vivo or whether it is formed during the purification of the enzyme. We have observed that the relative activity of $BSPAP_{ox}$ does increase significantly upon prolonged incubation of BSPAP with high amounts of zinc. For example, the activity of $BSPAP_{ox}$ relative to that of $BSPAP_{red}$ increased from 14% to 38% after incubation for 6 days at 22 °C in 5 mM zinc acetate, 50 mM sodium acetate, 2 M KCl, pH 5.0 (M. Merkx and B. A. Averill, unpublished results). Since no special precautions are normally taken during protein purification to maintain zinc-free conditions, we cannot exclude the possibility that the FeZn-BSPAP is formed during the purification. Beck et al. reported that the Zn^{2+} in FeZn-KBPAP can be exchanged for Fe^{2+} by incubation of the enzyme in excess ferrous ammonium sulfate (85 mM) and 2-mercaptoethanol (136 mM) for 40 h at 25 °C (*20*). The presence of manganese in the binuclear metal center in PP1 may also be the result of such a metal exchange process, as these enzymes are typically stored in manganese-containing buffers (*26*, *27*). The advantage of having zinc at the divalent metal site, as is found for KBPAP and protein phosphatase 2B, is the redox stability of the $Fe^{3+}Zn^{2+}$ cluster. A possible advantage of having Fe^{2+} at the divalent metal site, as is found in the mammalian purple acid phosphatases, is the possibility to control the activity of the enzyme by controlling its redox state. This redox switch model is supported by the fact that the product of the reaction, phosphate, enhances the oxidation and thus inactivates the enzyme. One might speculate that, to provide a low level of phosphatase activity under all conditions, it may be advantageous to also have a low level of FeZn enzymes.

ACKNOWLEDGMENT

We thank S. P. J. Albracht, A. J. Pierik, and W. Roseboom for assistance with the EPR spectroscopy, W. R. Hagen for allowing us to use the program RHOMBO, Y. Bruijn and M. Rijkenberg for doing some of the initial kinetics experi-

ments, and E. G. Funhoff and A. J. Pierik for critically reading the manuscript.

REFERENCES

1. Davis, J. C., and Averill, B. A. (1982) *Proc. Natl. Acad. Sci. U.S.A. 79*, 4623−4627.
2. Que, L., Jr., and True, A. E. (1990) *Prog. Inorg. Chem. 38*, 97−200.
3. Vincent, J. B., Olivier-Lilley, G. L., and Averill, B. A. (1990) *Chem. Rev. 90*, 1447−1467.
4. Wilcox, D. E. (1996) *Chem. Rev. 96*, 2435−2458.
5. Sträter, N., Lipscomb, W. N., Klabunde, T., and Krebs, B. (1996) *Angew. Chem., Int. Ed. Engl. 35*, 2024−2055.
6. Klabunde, T., and Krebs, B. (1997) *Struct. Bonding 89*, 177−198.
7. Chen, T. T., Bazer, F. W., Cetorelli, J. J., Pollard, W. E., and Roberts, R. M. (1973) *J. Biol. Chem. 248*, 8560−8566.
8. Campbell, H. D., and Zerner, B. (1973) *Biochem. Biophys. Res. Commun. 54*, 1498−1503.
9. Beck, J. L., McConachie, L. A., Summors, A. C., Arnold, W. N., de Jersey, J., and Zerner, B. (1986) *Biochim. Biophys. Acta 869*, 61−68.
10. Sugiura, Y., Kawabe, H., Tanaka, H., Fujimoto, S., and Ohara, A. (1981) *J. Biol. Chem. 256*, 10664−10670.
11. Hefler, S. K., and Averill, B. A. (1987) *Biochem. Biophys. Res. Commun. 146*, 1173−1177.
12. Jacobs, M. M., Nyc, J. F., and Brown, D. M. (1971) *J. Biol. Chem. 246*, 1419−1425.
13. Ullah, A. H. J., Mullaney, E. M., and Dischinger, H. C., Jr. (1994) *Biochem. Biophys. Res. Commun. 203*, 182−189.
14. Sinn, E., O'Connor, C. J., de Jersey, J., and Zerner, B. (1983) *Inorg. Chim. Acta 78*, L13−L15.
15. Debrunner, P. G., Hendrich, M. P., de Jersey, J., Keough, D. T., Sage, J. T., and Zerner, B. (1983) *Biochim. Biophys. Acta 745*, 103−106.
16. Keough, D. T., Dionysius, D. A., de Jersey, J., and Zerner, B. (1980) *Biochem. Biophys. Res. Commun. 94*, 600−605.
17. Beck, J. L., Keough, D. T., de Jersey, J., and Zerner, B. (1984) *Biochim. Biophys. Acta 791*, 357−363.
18. David, S. S., and Que, L., Jr. (1990) *J. Am. Chem. Soc. 112*, 6455−6463.
19. Beck, J. L., McArthur, M. J., de Jersey, J., and Zerner, B. (1988) *Inorg. Chim. Acta 153*, 39−44.
20. Beck, J. L., de Jersey, J., Zerner, B., Hendrich, M. P., and Debrunner, P. G. (1988) *J. Am. Chem. Soc. 110*, 3317−3318.
21. Sträter, N., Klabunde, T., Tucker, P., Witzel, H., and Krebs, B. (1995) *Science 268*, 1489−1492.
22. Klabunde, T., Sträter, N., Fröhlich, R., Witzel, H., and Krebs, B. (1996) *J. Mol. Biol. 259*, 737−748.
23. Klabunde, T., Sträter, N., Krebs, B., and Witzel, H. (1995) *FEBS Lett. 367*, 56−60.
24. Griffith, J. P., Kim, J. L., Kim, E. E., Sintchak, M. D., Thomson, J. A., Fitzgibbon, M. J., Fleming, M. A., Caron, P. R., Hsiao, K., and Navia, M. A. (1995) *Cell 82*, 507−522.
25. Kissinger, C. R., Parge, H. E., Knighton, D. R., Lewis, C. T., Pelletier, L. A., Tempczyk, A., Kalish, V. J., Tucker, K. D., Showalter, R. E., Moomaw, E. W., Gastinel, L. N., Habuka, N., Chen, X., Maldonado, F., Barker, J. E., Bacquet, R., and Villafranca, J. E. (1995) *Nature 378*, 641−644.
26. Goldberg, J., Huang, H.-B., Kwon, Y.-G., Greengard, P., Nairn, A. C., and Kuriyan, J. (1995) *Nature 376*, 745−753.
27. Egloff, M. P., Cohen, P. T. W., Reinemer, P., and Barford, D. (1995) *J. Mol. Biol. 254*, 942−959.
28. Koonin, E. V. (1994) *Protein Sci. 3*, 356−368.
29. Zhuo, S., Clemens, J. C., Stones, R. L., and Dixon, J. E. (1994) *J. Biol. Chem. 269*, 26234−26238.
30. Barton, G. J., Cohen, P. T. W., and Barford, D. (1994) *Eur. J. Biochem. 220*, 225−237.
31. Keough, D. T., Beck, J. L., de Jersey, J., and Zerner, B. (1982) *Biochem. Biophys. Res. Commun. 108*, 1643−1648.
32. Dietrich, M., Münstermann, D., Suerbaum, H., and Witzel, H. (1991) *Eur. J. Biochem. 199*, 105−113.
33. Wynne, C. J., Hamilton, S. E., Dionysius, D. A., Beck, J. L., and de Jersey, J. (1995) *Arch. Biochem. Biophys. 319*, 133−141.
34. Merkx, M., and Averill, B. A. (1998) *Biochemistry 37*, 8490−8497.
35. Rusnak, F., Yu, L., and Mertz, P. (1996) *J. Biol. Inorg. Chem. 1*, 388−396.
36. Wang, X., Culotta, V. C., and Klee, C. B. (1996) *Nature 383*, 434−437.
37. Yu, L., Haddy, A., and Rusnak, F. (1995) *J. Am. Chem. Soc. 117*, 10147−10148.
38. Yu, L., Golbeck, J., Yao, J., and Rusnak, F. (1997) *Biochemistry 36*, 10727−10734.
39. Mertz, P., Yu, L., Sikkink, R., and Rusnak, F. (1997) *J. Biol. Chem. 272*, 21296−21302.
40. Suerbaum, H., Körner, M., Witzel, H., Althaus, E., Mosel, B.-D., and Müller-Warmuth, W. (1993) *Eur. J. Biochem. 214*, 313−321.
41. Cammack, R., and Cooper, C. E. (1993) *Methods Enzymol. 227*, 353−384.
42. Hagen, W. R. (1992) *Adv. Inorg. Chem. 38*, 165−222.
43. Aasa, R., and Vänngård, T. (1975) *J. Magn. Reson. 19*, 308−315.
44. Albracht, S. P. J. (1984) *Curr. Top. Bioenerg. 13*, 79−106.
45. Pyrz, J. W., Sage, J. T., Debrunner, P. G., and Que, L., Jr. (1986) *J. Biol. Chem. 261*, 11015−11020.
46. Averill, B. A., Davis, J. C., Burman, S., Zirino, T., Sanders-Loehr, J., Loehr, T. M., Sage, J. T., and Debrunner, P. G. (1987) *J. Am. Chem. Soc. 109*, 3760−3767.
47. Aquino, M. A. S., Lim, J.-S., and Sykes, A. G. (1994) *J. Chem. Soc., Dalton Trans.*, 429−436.
48. Wang, D. L., Holz, R. C., David, S. S., Que, L., Jr., and Stankovich, M. T. (1991) *Biochemistry 30*, 8187−8194.
49. Vincent, J. B., Crowder, M. W., and Averill, B. A. (1991) *Biochemistry 30*, 3025−3034.
50. Crowder, M. W., Vincent, J. B., and Averill, B. A. (1992) *Biochemistry 31*, 9603−9608.
51. Vincent, J. B., Crowder, M. W., and Averill, B. A. (1991) *J. Biol. Chem. 266*, 17737−17740.
52. Antanaitis, B. C., Aisen, P., Lilienthal, H. R., Roberts, R. M., and Bazer, F. W. (1980) *J. Biol. Chem. 255*, 11204−11209.
53. Antanaitis, B. C., and Aisen, P. (1982) *J. Biol. Chem. 257*, 5330−5332.
54. Day, E. P., David, S. S., Peterson, J., Dunham, W. R., Bonvoison, J. J., Sands, R. H., and Que, L., Jr. (1988) *J. Biol. Chem. 263*, 15561−15567.
55. Gehring, S., Fleischhauer, P., Behlendorf, M., Hüber, M., Lorösch, J., Haase, W., Dietrich, M., Witzel, H., Löcke, R., and Krebs, B. (1996) *Inorg. Chim. Acta 252*, 13−17.
56. Wang, X., Randall, C. R., True, A. E., and Que, L., Jr. (1996) *Biochemistry 35*, 13946−13954.
57. Sage, J. T., Xia, Y.-M., Debrunner, P. G., Keough, D. T., de Jersey, J., and Zerner, B. (1989) *J. Am. Chem. Soc. 111*, 7239−7247.
58. Mueller, E. G., Crowder, M. W., Averill, B. A., and Knowles, J. R. (1993) *J. Am. Chem. Soc. 115*, 2974−2975.
59. Kauzlarich, S. M., Teo, B. K., Zirino, T., Burman, S., Davis, J. C., and Averill, B. A. (1986) *Inorg. Chem. 25*, 2781−2785.
60. True, A. E., Scarrow, R. C., Randall, C. R., Holz, R. C., and Que, L., Jr. (1993) *J. Am. Chem. Soc. 115*, 4246−4255.

BI980389R